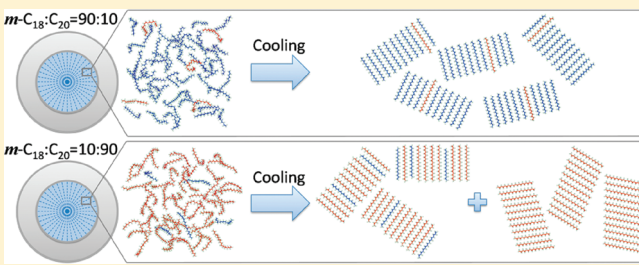


Crystallization Behavior of Binary Even–Even *n*-Alkane Mixtures in Microcapsules: Effect of Composition and Confined Geometry on Solid–Solid phase Separation

Dongsheng Fu,^{†,‡} Yufeng Liu,[†] Yunlan Su,^{*,†} Guoming Liu,^{†,‡} and Dujin Wang^{*,†}[†]Beijing National Laboratory for Molecular Sciences, Key Laboratory of Engineering Plastics, Institute of Chemistry, Chinese Academy of Sciences, Beijing 100190, China[‡]Graduate University of Chinese Academy of Sciences, Beijing 100190, China

ABSTRACT: The crystallization behaviors of binary even–even normal alkane (*n*-alkane) mixtures (*n*-C₁₈H₃₈/*n*-C₂₀H₄₂, abbreviated as C₁₈/C₂₀) with different compositions, both in the bulk state and in nearly monodisperse microcapsules, have been investigated by the combination of differential scanning calorimetry and temperature-dependent X-ray diffraction. The solid–solid phase separation, usually observed during the cooling process of bulk samples, is greatly suppressed and even eliminated after being microencapsulated, with the orthorhombic-ordered phase dominating in the low-temperature crystal.

Such a crystallization transition is attributed to the special interaction between the two even *n*-alkanes and the confined environment in microcapsules. The triclinic ordered phase, solely formed by the single even *n*-alkanes (C₁₈ or C₂₀), becomes less stable due to the weakening of the layered structure and the suppression of the terminal methyl–methyl interactions in the confined geometry, which favors the miscibility of the two components. Furthermore, besides the chain-length difference and the composition, the confined environment is proved to be another important factor to exert strong positive influence on suppressing the solid–solid phase separation of C₁₈/C₂₀ binary system.



INTRODUCTION

Long-chain normal alkanes (*n*-C_{*n*}H_{2*n*+2}, abbreviated as C_{*n*}), bearing the linear chain molecular structure, often serve as the most essential building blocks of organic, biological, and polymeric systems.¹ Bulk *n*-alkanes have some unique features in phase transition processes such as the surface freezing phenomenon,^{2,3} rotator phases⁴ and odd–even effect in the low-temperature ordered crystal.⁵ The surface freezing phenomenon means that a surface crystalline monolayer is formed at the temperature of up to ~3 °C above the bulk crystallization temperature, which is stacked into a planar hexagonal phase, and exerts strong influence on the formation of the bulk solid phases. The rotator phases exist between isotropic liquid state and the low-temperature ordered crystal, exhibiting long-range order in the molecular axis orientation and the center of mass position but lacking long-range order in the rotational degree of freedom of the molecules around their long axis. The odd–even effect is described as that at low temperatures, even alkanes crystallize into triclinic form while odd ones crystallize into orthorhombic. Compared to bulk *n*-alkanes, the mixtures of these materials are more prevalent in practical applications such as the phase change materials (PCMs) and useful models for the polydisperse polymethylene chain packing found in polyethylene lamellae as well as the mixed acyl chain layers in biological lipids. Therefore, these mixtures have been extensively investigated

using both experimental methodologies and theoretical simulations.^{6–12} It has been recognized that mixing alkanes with different chain lengths leads to dramatic influence on the phase behaviors of the mixtures. This kind of mixing reduces the interaction of interlayer coupling, increasing void volume and lamellar surface roughness, thus enhancing the stability of rotator phases, and correspondingly, the odd–even effect disappears in *n*-alkane mixtures.¹³ Binary *n*-alkane mixtures have been proven to undergo a phase separation process in low-temperature ordered crystals, and thus they are important models for understanding the crystallization behavior of petroleum waxes and other mixed solid phases of chain molecules. One of the major factors that can greatly affect the phase separation is the chain-length difference.¹⁴ For binary mixtures, the phase separation is expected to emerge if the longer chain-length carbon number is 1.22 times as many as the number of carbons in the shorter chain.¹³ That is, if the chain-length difference of a mixture is 3 or 4 carbons, it usually undergoes a detectable phase separation under all compositions.¹⁴ Binary *n*-alkane mixtures with this certain chain-length difference have been widely investigated, and many novel phase behaviors have been observed and even

Received: January 15, 2011

Revised: March 11, 2011

Published: April 05, 2011

computer-simulated.^{15–18} Up to date, however, there are few reports focusing on the mixtures formed by components with smaller carbon number and chain-length difference. Furthermore, as another fundamental factor, the composition can also exert remarkable influence on the phase separation of binary *n*-alkane mixtures with small chain-length difference, yet the attempts to develop an in-depth understanding of the two aspects above have not been presented.

More recently, novel rotator phases and anomalous nucleation kinetics were observed for *n*-alkanes and their mixtures confined in emulsified microdroplets,^{19–21} microcapsules,^{22,23} and mesoporous silica matrix or mesopores.^{24–26} It has been shown that the phase separation of simple fluids in porous media^{27,28} and polymer blends in thin film is suppressed,^{29,30} which is attributed to the confinement effect. It would thus be of interest to learn how geometrical confinement affects the phase separation of binary *n*-alkane mixtures. Previously, we investigated the mixture of odd–even *n*-alkanes in nearly monodisperse microcapsules^{31,32} and found that the solid–solid phase separation at low temperature, which is originally manifest in the bulk *n*-alkane mixtures, was proved to be totally suppressed in the microencapsules.³² In addition to the odd–even system, one can expect more fascinating results on confined binary *n*-alkane mixtures consisting of two even *n*-alkanes with the chain-length difference of two carbons. Two aspects are considered for the investigation of the even–even *n*-alkane binary mixture in confined geometry. (1) It is interesting to make it clear whether orthorhombic structure, which has been confirmed to be the most stable low-temperature crystal phase in all bulk *n*-alkane mixtures, will still dominate in even–even *n*-alkane system in confined geometry, and (2) the least chain-length difference in the even–even *n*-alkane binary mixture is two carbons, which enlarges the interaction difference between the two components and will dramatically affect the phase behaviors of the mixtures. Hence, it is quite essential to investigate such an important system of the binary even–even *n*-alkane mixture.

In the former reports, we have shown that unique three-dimensional confinement of microcapsules provides an exhilarating opportunity for the research on the phase separation behaviors of an odd–even *n*-alkane mixture consisting of *n*-C₁₈H₃₈ (C₁₈) and *n*-C₁₉H₄₀ (C₁₉).³² In the present work, we focus on the phase separation of two even *n*-alkanes, *n*-C₁₈H₃₈ and *n*-C₂₀H₄₂ (abbreviated as C₁₈/C₂₀), under different compositions both in the bulk state and in microcapsules. A similar elimination of phase separation in microencapsulated C₁₈/C₂₀ = 90/10 (abbreviated as *m*-C₁₈/C₂₀ = 90/10) like the previous microencapsulated C₁₈/C₁₉ = 90/10 (*m*-C₁₈/C₁₉ = 90/10) was observed. However, the phase separation could survive in microencapsulated C₁₈/C₂₀ = 10/90 (*m*-C₁₈/C₂₀ = 10/90). An illustration scheme has been proposed to explain the confinement effect on phase separation behaviors of binary *n*-alkane mixtures in terms of the crystal structure and packing mode of alkane molecules.

■ EXPERIMENTAL METHODS

n-C₂₀H₄₂ (purity >99%) and *n*-C₁₈H₃₈ (purity >99%) were purchased from Acros Company, and all compounds were used as received. The solid bulk components were weighted in the desired molar fractions and melting-mixed. Using melamine-formaldehyde (M-F) resin as the shell material and *n*-alkane mixtures as the core material, microcapsules were prepared by

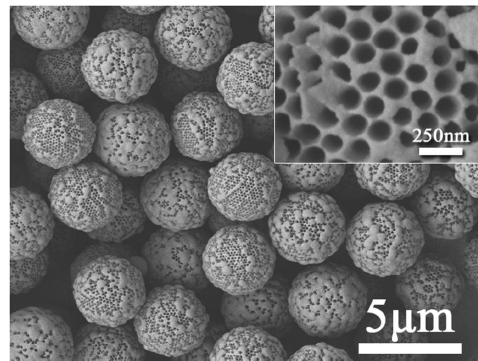


Figure 1. SEM micrographs of microcapsules containing *n*-alkane mixtures prepared by in situ polymerization of melamine-formaldehyde, with 4-(1,1,3,3-tetramethylbutyl) phenyl-polyethylene glycol (Triton X-100) as emulsifier. The inset is the high-magnification image.

in situ polymerization according to literatures.^{33,34} This method provides us with nearly monodisperse and highly heat-resistant microcapsules, inside which *n*-alkane mixtures were confined to individually small microdomains surrounded by the noncrystalline wall of M-F resin.

The particle size and surface morphology of the prepared microcapsules were examined by a JEOL-JSM-6700F scanning electron microscope (SEM) (Figure 1), fitted with a field emission source and operated at an accelerating voltage of 5 kV. The differential scanning calorimetry (DSC) measurements were carried out on a Perkin-Elmer DSC7 calorimeter at a cooling/heating rate of 2 °C/min. Specimens were heated from room temperature to 45 °C and then cooled down to –10 °C, followed by heating again to 45 °C. The first cooling and second heating thermograms were recorded.

Temperature-dependent X-ray diffraction (XRD) experiments were performed on an Pert Pro MPD X-ray diffractometer over the temperature range from –10 to 45 °C, using Cu K α radiation (1.54 Å), power of 40 mA/40 kV, and rotating angle $2\theta = 5\text{--}40^\circ$. The samples with thickness of about 1 mm were enclosed in aluminum foil, first heated from room temperature to 45 °C, kept for 5 min, and followed by cooling to –10 °C. The heating and cooling rates were all 2 °C/min, and at each temperature point, the samples were equilibrated for about 5 min before measurements.

■ RESULTS AND DISCUSSION

Phase Transition Behaviors of C₁₈/C₂₀ Mixtures in Both Bulk and Microencapsulated States. 1. C₁₈/C₂₀ = 90/10. Figure 2 shows the crystallization behaviors of C₁₈/C₂₀ = 90/10 (weight ratio) both in the bulk (upper line) and microencapsulated states (lower line). For the bulk C₁₈/C₂₀ = 90/10 (abbreviated as *b*-C₁₈/C₂₀ = 90/10), a big exothermic peak appearing at 26.5 °C corresponds to the liquid-rotator transition. Another peak is observed at 4.2 °C, which is regarded as the transition from the rotator to the low-temperature crystal. For the *m*-C₁₈/C₂₀ = 90/10, however, two extra exothermic peaks (see the two arrows in Figure 2) can be found during the cooling process. First, a small sharp exothermic peak emerges above the freezing temperature of about 3 °C, corresponding to the surface freezing.^{22,23,31,32} Second, a shoulder exothermic peak appears just below the liquid-rotator transition, indicating a probable new phase transition that is absent in the bulk sample.

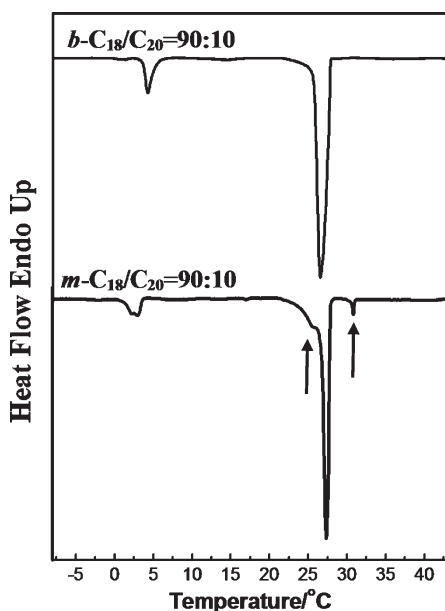


Figure 2. DSC curves of $b\text{-C}_{18}/\text{C}_{20} = 90:10$ (upper line) and $m\text{-C}_{18}/\text{C}_{20} = 90:10$ (lower line) during the cooling process. Black arrows indicate the two new exothermic peaks in the $m\text{-C}_{18}/\text{C}_{20} = 90:10$ system.

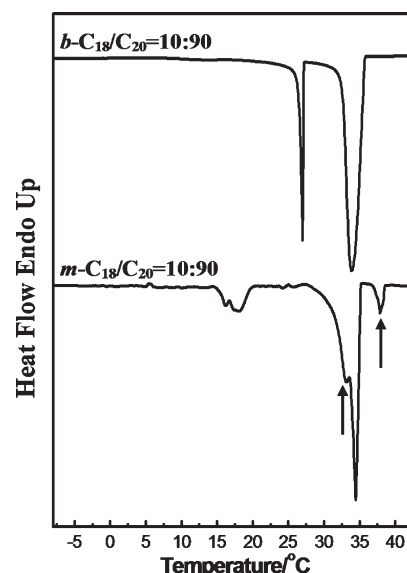


Figure 4. DSC traces of $b\text{-C}_{18}/\text{C}_{20} = 10:90$ (upper line) and $m\text{-C}_{18}/\text{C}_{20} = 10:90$ (lower line) during the cooling process. Black arrows indicate the two new exothermic peaks in the $m\text{-C}_{18}/\text{C}_{20} = 10:90$ system.

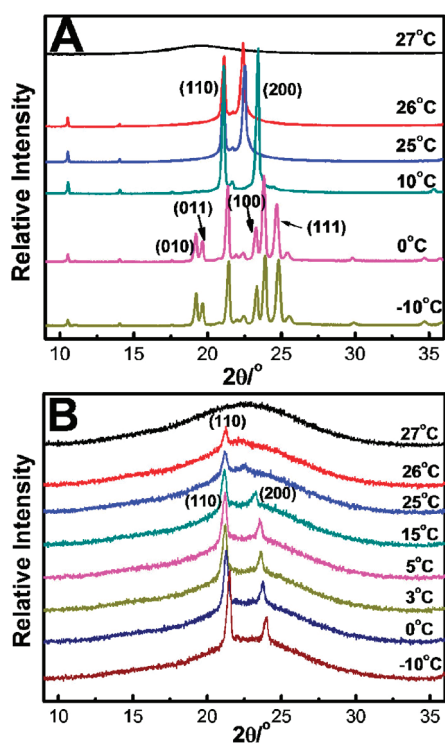


Figure 3. Temperature-dependent XRD patterns of $\text{C}_{18}/\text{C}_{20} = 90/10$ at selected temperatures during the cooling process: (A) bulk sample and (B) microencapsulated sample. The cooling rate was $2\text{ }^{\circ}\text{C}/\text{min}$.

To further characterize the crystal structures and phase transitions during the crystallization process of both specimens, temperature-dependent XRD measurements were performed, as shown in Figure 3. It is observed that above $27\text{ }^{\circ}\text{C}$, the two samples all exist in the isotropic liquid state, characterized by a

single halo at $2\theta = 22^{\circ}$. For the $b\text{-C}_{18}/\text{C}_{20} = 90/10$ (Figure 3A), with temperature decreasing to $26\text{ }^{\circ}\text{C}$ two characteristic peaks of (110) and (200) appear, corresponding to the orthorhombic rotator phase I (RI).^{4,5,25} With temperature decreasing to $0\text{ }^{\circ}\text{C}$, four characteristic diffraction peaks of (010), (100), (011), and (111) emerge, corresponding to the triclinic phase,⁵ while the characteristic diffraction peak of (110) for orthorhombic phase still remains. This indicates that an obvious phase separation occurs at $0\text{ }^{\circ}\text{C}$ in $b\text{-C}_{18}/\text{C}_{20} = 90/10$. Compared to $b\text{-C}_{18}/\text{C}_{20} = 90/10$, one characteristic peak of (110) for the rhombohedral rotator phase (RII) is observed in $m\text{-C}_{18}/\text{C}_{20} = 90/10$ with the sample cooling down to $26\text{ }^{\circ}\text{C}$ (Figure 3B), which is assigned to the small exothermic peak below the liquid-rotator transition according to the DSC data.²² As the sample was further cooled down to $25\text{ }^{\circ}\text{C}$, two characteristic peaks of (110) and (200) for the orthorhombic phase are observed, indicating a rotator–rotator transition from RII to RI. The triclinic phase, however, does not appear in the microencapsulated sample within the whole temperature range, and therefore the orthorhombic rotator phase (RI) is translated directly into the stable orthorhombic phase, instead of fractionating into two phases like those of the bulk sample (triclinic and orthorhombic). The distinct difference of the phase behavior between $b\text{-C}_{18}/\text{C}_{20} = 90/10$ and $m\text{-C}_{18}/\text{C}_{20} = 90/10$ illustrates that confined geometry eliminates the chain-length difference between the two components, making them form a unique solid solution.³²

$2\text{-C}_{18}/\text{C}_{20} = 10/90$. Compared to the $\text{C}_{18}/\text{C}_{20} = 90/10$ ($\bar{n} = 18.2$), the average chain length in the sample of $\text{C}_{18}/\text{C}_{20} = 10/90$ ($\bar{n} = 19.8$) is longer and the phase behavior of the bulk state is similar to $n\text{-C}_{20}\text{H}_{42}$ (not shown here), as shown in the upper line of Figure 4. The $b\text{-C}_{18}/\text{C}_{20} = 10/90$ is first trapped into a rotator phase at $33.9\text{ }^{\circ}\text{C}$ and then converts to the stable low-temperature crystal at $27\text{ }^{\circ}\text{C}$. As for the $m\text{-C}_{18}/\text{C}_{20} = 10/90$, two more exothermic peaks emerge during the crystallization process, showing a similar situation as the $m\text{-C}_{18}/\text{C}_{20} = 90/10$ (Figure 4, lower line). A small sharp peak above the freezing

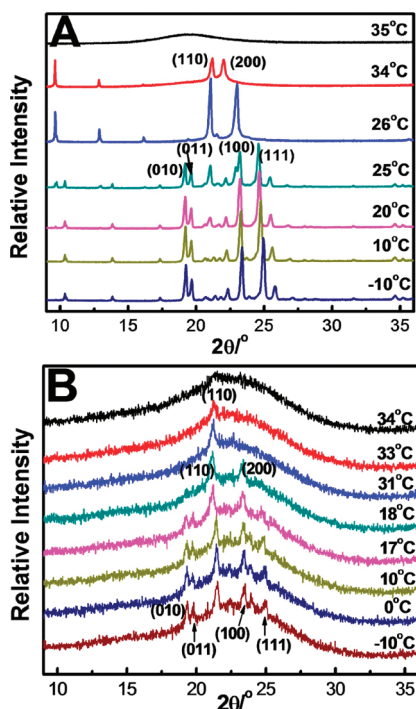


Figure 5. Temperature-dependent XRD results of $C_{18}/C_{20} = 10/90$ at selected temperatures during the cooling process: (A) bulk sample and (B) microencapsulated sample. The cooling rate was $2\text{ }^{\circ}\text{C}/\text{min}$.

temperature of about $3\text{ }^{\circ}\text{C}$ (surface freezing) and a shoulder one just below the liquid-rotator transition are observed.

The temperature-dependent XRD results (Figure 5) are consistent with those temperatures of phase transition measured by DSC. As shown in Figure 5A, with cooling the $b\text{-}C_{18}/C_{20} = 10/90$ sample to $34\text{ }^{\circ}\text{C}$ two characteristic peaks of (110) and (200) appear, corresponding to the orthorhombic RI. With temperature decreasing to $25\text{ }^{\circ}\text{C}$, four characteristic diffraction peaks of (010), (100), (011) and (111) for the triclinic phase, emerge. Meanwhile, the (110) peak for the orthorhombic phase does not disappear, which indicates an obvious phase separation at $25\text{ }^{\circ}\text{C}$ in $b\text{-}C_{18}/C_{20} = 10/90$. However, unlike the situation for $b\text{-}C_{18}/C_{20} = 90/10$ (Figure 3A), the (110) peak for $b\text{-}C_{18}/C_{20} = 10/90$ is weakened with temperature decreasing and almost disappears below $10\text{ }^{\circ}\text{C}$. After being microencapsulated, a single peak of (110) indicates the appearance of the rhombohedral RI at $33\text{ }^{\circ}\text{C}$ for the $m\text{-}C_{18}/C_{20} = 10/90$ (Figure 5B). With cooling the sample to $31\text{ }^{\circ}\text{C}$, the characteristic peak of (200) emerges, indicating that the mixture has been trapped into the orthorhombic RI. With temperature further decreasing to $17\text{ }^{\circ}\text{C}$, the characteristic peaks of the triclinic phase appear, indicating that the phase separation still exists in the microencapsulated sample, not the same as the $m\text{-}C_{18}/C_{20} = 90/10$ (Figure 3B). The present observation is obviously different from the previous report that the phase separation in $m\text{-}C_{18}/C_{19}$ mixture can be totally suppressed by the confinement effect,³² which implies that the phase change mechanisms for even–even and odd–even *n*-alkane mixtures are not the same.

Crystal Structure and Interlayer Coupling of C_{18}/C_{20} Mixtures in Both Bulk and Microencapsulated States. For the bulk *n*-alkane mixtures, the phenomenon of phase separation can be usually observed in the temperature range of the low-temperature ordered phase.^{14–16} It has been known that the

chain-length difference and the composition are the major factors governing the phase separation behavior. The larger the chain-length difference is, the stronger the phase separation behaves, and the more extensive range of the composition the phase separation will cover. Compared to the previous odd–even system,³² the even–even *n*-alkane mixture has a larger chain-length difference. Therefore, it is expected that the phase separation will be more enhanced in the bulk state. Such speculation seems to be consistent with the experimental results shown in Figures 3A and 5A, where phase separation is manifestly illustrated that the orthorhombic ordered phase coexists with the triclinic ordered phase in a long temperature range for two bulk samples. However, there are some differences for the phase transitions between the two compositions. For $b\text{-}C_{18}/C_{20} = 90/10$, the phase separation still exists even at $-10\text{ }^{\circ}\text{C}$ (Figure 3A). Since both of the components are the even *n*-alkanes with the triclinic crystal as their low-temperature ordered phase,⁵ the orthorhombic phase in this binary even–even *n*-alkane mixture must be formed by the combination of the two components on molecular level. Therefore, the phase separation feature of $b\text{-}C_{18}/C_{20} = 90/10$ is that the orthorhombic ordered phase formed by the two components coexists with the triclinic phase formed by single C_{18} . The situation in $b\text{-}C_{18}/C_{20} = 10/90$, however, is different to a great extent. At the very beginning of the phase separation as shown in Figure 5A, the characteristic peak of (110) corresponding to the orthorhombic ordered phase is obvious, indicating the coexistence of the two ordered phases. But with temperature decreasing, this peak is gradually weakened and almost disappears below $10\text{ }^{\circ}\text{C}$, which means that the orthorhombic ordered phase is nearly nonexistent. The disappearance of the orthorhombic phase formed by the two components in this binary even–even *n*-alkane mixture illuminates the complete phase separation of the two components of $b\text{-}C_{18}/C_{20} = 10/90$. Therefore, the triclinic ordered phase in this sample comprises in fact two phases, which are crystallized separately by the two components into their own low-temperature stable crystal form (triclinic).

The previous report showed that for the bulk binary odd–even *n*-alkane mixture under a certain composition, the phenomenon of the phase separation can also be observed, however, after microencapsulation, the phase separation is fully suppressed (e.g., $m\text{-}C_{18}/C_{19} = 90/10$).³² Similar results have been obtained in the $m\text{-}C_{18}/C_{20} = 90/10$ sample (Figure 3B). The only existing phase at low temperature is the orthorhombic ordered phase, characterized by the double characteristic peaks of (110) and (200), while the triclinic phase is absent. It has been reported that the restricted geometry can exert strong influence on the packing arrangement of the solid condensate such as the *n*-alkanes and some molecules (O_2 , Ar, etc.), which adapts to the confinement by forming a 2D close-packed structure with lattice defects and lattice strains.^{26,35} For the $m\text{-}C_{18}/C_{20} = 90/10$ sample, the low-angle series of (002), (004), and (006) reflections, which can be observed in its bulk counterpart (Figure 3A), is greatly weakened in the confined geometry, as shown in Figure 3B. The weakening of (00l) reflections from the diffraction patterns of $m\text{-}C_{18}/C_{20} = 90/10$ implies the positional disorder along the crystallographic *c*-axis (carbon chain).^{24–26} Namely, the layered structure is partially suppressed due to the confinement effect, which directly changes the relative stability of the orthorhombic or triclinic ordered phases. In the low-temperature ordered phases of the *n*-alkanes, there are two interactions, terminal methyl–methyl ($\text{CH}_3\text{--CH}_3$) interactions

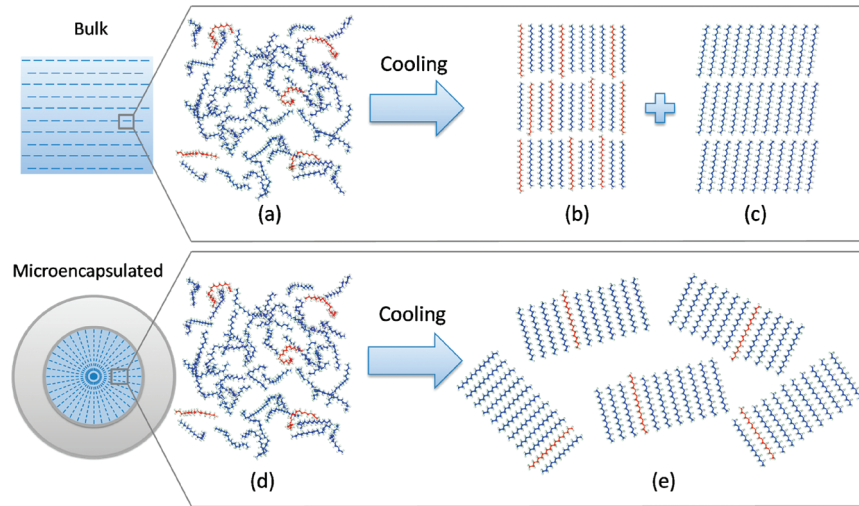


Figure 6. Schematic illustration of the crystal structure and interlayer arrangement of $b\text{-C}_{18}/\text{C}_{20} = 90/10$ (upper part) and $m\text{-C}_{18}/\text{C}_{19} = 90/10$ (lower part). For $b\text{-C}_{18}/\text{C}_{20} = 90/10$, the isotropic liquid state (a) is transferred into the coexistence of orthorhombic (b) and triclinic (c, solely by C_{18}) ordered phases. For $m\text{-C}_{18}/\text{C}_{20} = 90/10$, the isotropic liquid state (d) is transferred only into orthorhombic ordered phase (e).

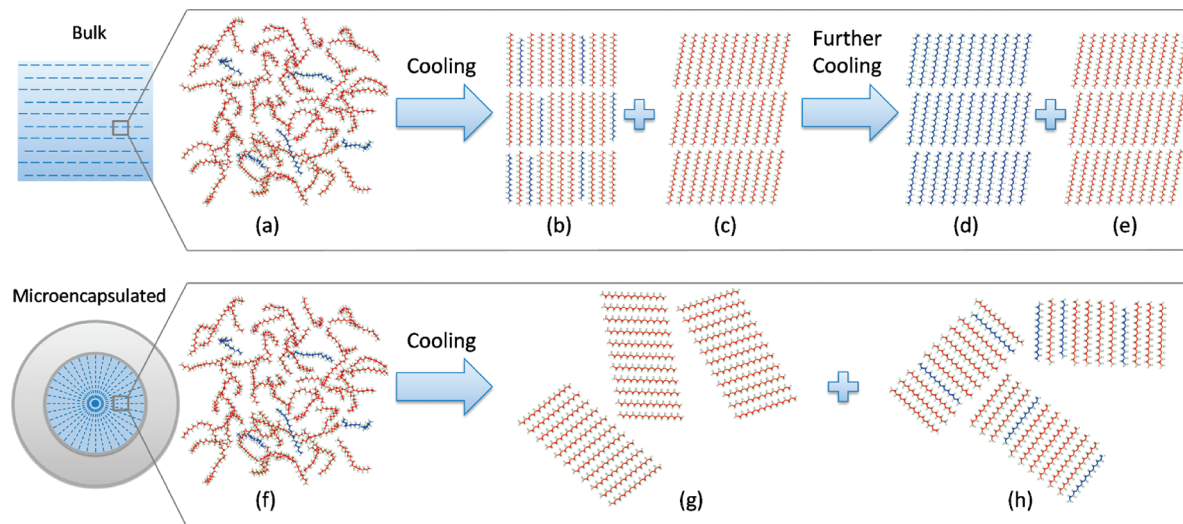


Figure 7. Schematic illustration of the crystal structure and interlayer arrangement of $b\text{-C}_{18}/\text{C}_{20} = 10/90$ (upper part) and $m\text{-C}_{18}/\text{C}_{19} = 10/90$ (lower part). For $b\text{-C}_{18}/\text{C}_{20} = 10/90$, the isotropic liquid state (a) is transferred into the coexistence of orthorhombic (b) and triclinic (c, solely by C_{20}) ordered phases; with temperature further decreasing, the triclinic crystal exists separately by the two components, C_{18} (d) and C_{20} (e). For $m\text{-C}_{18}/\text{C}_{19} = 10/90$, the isotropic liquid state (f) is transferred into the coexistence of triclinic (g, solely by C_{20}) and orthorhombic (h) ordered phases.

between the adjacent layers and the methylene–methylene ($\text{CH}_2\text{—CH}_2$) intermolecular interactions within the layers.³⁶ For the bulk even *n*-alkanes with shorter chain length ($n < 26$), the layered structure favors the terminal methyl groups packing in the opposite directions at the layer interfaces. The terminal $\text{CH}_3\text{—CH}_3$ interactions dominate the solid–solid packing resulting in a preferred unimolecular triclinic crystal lattice, and thus the triclinic phase is the stable crystal phase.³⁷ For $b\text{-C}_{18}/\text{C}_{20} = 90/10$, the isotropic liquid phase (Figure 6a) transfers to RI then to the ordered crystal phase. The terminal $\text{CH}_3\text{—CH}_3$ interactions are greatly weakened due to the chain-length difference, since only low amount of C_{20} with longer chain length can easily destroy the layered structure. Therefore, the $\text{CH}_2\text{—CH}_2$ intermolecular interactions become dominant, and the formation of an orthogonal unit cell is preferred, leading

to the favored orthorhombic ordered phase (Figure 6b). Nevertheless, the amount of C_{20} is too small to affect all the amount of C_{18} , and hence C_{18} crystallizes separately into the triclinic ordered phase in the area without C_{20} (Figure 6c). In the $m\text{-C}_{18}/\text{C}_{20} = 90/10$, the liquid state is regarded the same as in the bulk sample (Figure 6d). However, the layered structure of low-temperature crystal phases is partially suppressed, which further weakens the terminal $\text{CH}_3\text{—CH}_3$ interactions, causing the triclinic ordered phase more unstable. Furthermore, it can be reasonably speculated that the weakening of the layered structure facilitates the longitudinal chain diffusion, causing C_{20} better dispersed than in the bulk state. Therefore, the greatly reduced stability of the triclinic ordered phase and the better dispersion of C_{20} in $m\text{-C}_{18}/\text{C}_{20} = 90/10$ are combined to eliminate the phase separation originally shown in $b\text{-C}_{18}/\text{C}_{20} =$

90/10, so that the orthorhombic ordered phase is dominant (Figure 6e).

The situation in the $m\text{-C}_{18}/\text{C}_{20} = 10/90$, however, is not the same as that in the $m\text{-C}_{18}/\text{C}_{20} = 90/10$. Phase separation can be clearly observed since the characteristic peak of (110) for the orthorhombic ordered phase formed by the combination of the two components still emerges even at very low temperature (Figure 5B), which indicates that the total separation of the two components in $b\text{-C}_{18}/\text{C}_{20} = 10/90$ is suppressed in the confinement. The appearance of the orthorhombic phase at low temperature implies that there must be some region filled with both components on molecular level and the C_{20} fails to entirely exclude the C_{18} from its crystal lattice in the confinement. For $b\text{-C}_{18}/\text{C}_{20} = 10/90$, the isotropic liquid phase (Figure 7a) also transfers to RI then to the ordered crystal phase, and the orthorhombic-ordered phase (Figure 7b) coexists with the triclinic phase (Figure 7c) just after the rotator-crystal transition. The terminal CH_3-CH_3 interactions in the ordered crystal phase are also weakened due to the chain-length difference, but this weakness is not as strong as that for $b\text{-C}_{18}/\text{C}_{20} = 90/10$. However, since the C_{18} with a shorter chain length is the minor component, the triclinic crystal lattice of the C_{20} will be less affected by the mixing, and the C_{18} molecules can be easily excluded from the crystal lattice of C_{20} , leading to the complete separation of the two components (Figure 7d,e). For $m\text{-C}_{18}/\text{C}_{20} = 10/90$, the isotropic liquid state is also regarded the same as that in the bulk sample (Figure 7f), and the layered structure of ordered phases is also weakened, which accelerates the longitudinal chain diffusion and promotes the mixing. However, as the C_{18} cannot strongly destroy the triclinic crystal lattice of C_{20} , the triclinic ordered phase formed by C_{20} can be preserved (Figure 7g). Meanwhile, some C_{20} with C_{18} crystallizes into orthorhombic ordered phase, characterized by the (110) peak under low temperature (Figure 7h). Because of the better dispersion of C_{18} and not strongly reduced stability of the triclinic ordered phase in $m\text{-C}_{18}/\text{C}_{20} = 10/90$, the phase separation is partially suppressed, and the coexistence of two kinds of ordered phases is observed instead of the total separation of the two components in $b\text{-C}_{18}/\text{C}_{20} = 10/90$.

As mentioned above, microencapsulation can exert prominent effect on the phase behavior of binary even–even *n*-alkane mixtures. Besides, other confinement such as thin films and emulsified microdroplets can also affect the phase behaviors and crystallization kinetics of other condensed matters.^{24–30} Therefore, in addition to the chain-length difference and the composition, suitable confinement can be regarded as another important factor that determines the phase separation and other phase behaviors of the *n*-alkane mixtures. Furthermore, the present work on the phase separation of the confined *n*-alkane solid solutions can be propitious to better understand the phase change mechanism of PCMs containing confined *n*-alkanes and shed some new lights on designing and preparing this kind of PCMs.

CONCLUSIONS

In summary, we have investigated the phase separation behavior of the bulk binary even–even *n*-alkane mixtures ($b\text{-C}_{18}/\text{C}_{20}$) and microencapsulated counterparts ($m\text{-C}_{18}/\text{C}_{20}$) with different compositions. Phase separation can be found in both $b\text{-C}_{18}/\text{C}_{20} = 90/10$ and $b\text{-C}_{18}/\text{C}_{20} = 10/90$, where two ordered phases (orthorhombic and triclinic) coexist in low

temperature crystals. With temperature further decreasing, however, orthorhombic phase nearly disappears in $b\text{-C}_{18}/\text{C}_{20} = 10/90$, since C_{18} can be easily excluded from the crystal lattice of C_{20} , and finally triclinic ordered phase is co-formed by separately crystalline C_{18} and C_{20} . In microcapsules, the weakening of the layered structure and the terminal methyl–methyl interactions due to the confinement plays an important role in suppressing the phase separation. The $m\text{-C}_{18}/\text{C}_{20} = 90/10$ sample only transforms into one stable orthorhombic phase, showing a total elimination of phase separation. In $m\text{-C}_{18}/\text{C}_{20} = 10/90$, the triclinic ordered phase coexists with the orthorhombic ordered phase, showing a partially suppression of the phase separation. These findings may shed new lights on understanding the phase separation of other mixed systems such as waxes, lipids, and polymer blends in confined geometry.

AUTHOR INFORMATION

Corresponding Author

*Phone: +86-10-82618533. Fax: +86-10-82612857. E-mail: (Y.S.) ylsu@iccas.ac.cn; (D.W.) djwang@iccas.ac.cn.

ACKNOWLEDGMENT

We thank the National Natural Science Foundation of China (50573086) and China National Funds for Distinguished Young Scientists (Grant 50925313) for financial support.

REFERENCES

- (1) Small, D. M. *The Physical Chemistry of Lipids*; Plenum: New York, 1986.
- (2) Ocko, B. M.; Wu, X. Z.; Sirota, E. B.; Sinha, S. K.; Gang, O.; Deutsch, M. *Phys. Rev. E* **1997**, *55*, 3164–3182.
- (3) Wu, X. Z.; Ocko, B. M.; Sirota, E. B.; Sinha, S. K.; Deutsch, M.; Cao, B. H.; Kim, M. W. *Science* **1993**, *261*, 1018–1021.
- (4) Sirota, E. B.; Singer, D. M. *J. Chem. Phys.* **1994**, *101*, 10873–10882.
- (5) Dirand, M.; Bouroukba, M.; Chevallier, V.; Petitjean, D. *J. Chem. Eng. Data* **2002**, *47*, 115–143.
- (6) Asbach, G. I.; Kilian, H. G.; Stacke, F. *Colloid Polym. Sci.* **1982**, *260*, 151–163.
- (7) Bonsor, D. H.; Bloor, D. *J. Mater. Sci.* **1977**, *12*, 1559–1564.
- (8) Craievich, A.; Doucet, J.; Denicolò, I. *J. Phys. (Paris)* **1984**, *45*, 1473–1477.
- (9) Denicolò, I.; Craievich, A. F.; Doucet, J. *J. Chem. Phys.* **1984**, *80*, 6200–6203.
- (10) Kitaigorodskii, A. I.; Mnyukh, Yu. V.; Nechitailo, N. A. *Sov. Phys. Crystallogr.* **1958**, *3*, 303–308.
- (11) Luth, H.; Nyburg, S. C.; Robinson, P. M.; Scott, H. G. *Mol. Cryst. Liq. Cryst.* **1974**, *27*, 337–357.
- (12) Maroncelli, M.; Strauss, H. L.; Snyder, R. G. *J. Phys. Chem.* **1985**, *89*, 5260–5267.
- (13) Sirota, E. B.; King, H. E.; Shao, H. H.; Singer, D. M. *J. Phys. Chem.* **1995**, *99*, 798–804.
- (14) Snyder, R. G.; Clavell-Grunbaum, D.; Strauss, H. L. *J. Phys. Chem. B* **2007**, *111*, 13957–13966.
- (15) Dorset, D. L. *Macromolecules* **1987**, *20*, 2782–2788.
- (16) Dorset, D. L.; Snyder, R. G. *J. Phys. Chem. B* **1999**, *103*, 3282–3286.
- (17) Annis, B. K.; Londono, J. D.; G. D. Wignall, R. G. *J. Phys. Chem.* **1996**, *100*, 1725–1730.
- (18) Hacura, A.; Kaczorowska, B. *J. Mol. Struct.* **2005**, *744*, 581–584.
- (19) Montenegro, R.; Antonietti, M.; Mastai, Y.; Landfester, K. *J. Phys. Chem. B* **2003**, *107*, 5088–5094.

- (20) Herhold, A. B.; Ertas, D.; Levine, A. J.; King, H. E. *Phys. Rev. E* **1999**, *59*, 6946–6955.
- (21) Herhold, A. B.; King, H. E.; Sirota, E. B. *J. Chem. Phys.* **2002**, *116*, 9036–9050.
- (22) Xie, B. Q.; Shi, H. F.; Jiang, S. C.; Zhao, Y.; Han, C. C.; Xu, D. F.; Wang, D. J. *J. Phys. Chem. B* **2006**, *110*, 14279–14282.
- (23) Xie, B. Q.; Shi, H. F.; Liu, G. M.; Zhou, Y.; Wang, Y.; Zhao, Y.; Wang, D. J. *J. Phys. Chem. B* **2008**, *112*, 13310–13315.
- (24) Henschel, A.; Hofmann, T.; Huber, P.; Knorr, K. *Phys. Rev. E* **2007**, *75*, 021607.
- (25) Huber, P.; Sopranyuk, V. P.; Knorr, K. *Phys. Rev. E* **2006**, *74*, 031610.
- (26) Huber, P.; Wallacher, D.; Albers, J.; Knorr, K. *Europhys. Lett.* **2004**, *65*, 351–357.
- (27) Alba-Simionescu, C.; Coasne, B.; Dosseh, G.; Dudziak, G.; Gubbins, K. E.; Radhakrishnan, R.; Sliwinska-Bartkowiak, M. *J. Phys.: Condens. Mat.* **2006**, *18*, R15–R68.
- (28) Gelb, L. D.; Gubbins, K. E.; Radhakrishnan, R.; Sliwinska-Bartkowiak, M. *Rep. Prog. Phys.* **1999**, *62*, 1573–1659.
- (29) Sung, L.; Karim, A.; Douglas, J. F.; Han, C. C. *Phys. Rev. Lett.* **1996**, *76*, 4368–4371.
- (30) Akpalu, Y. A.; Karim, A.; Satija, S. K.; Balsara, N. P. *Macromolecules* **2001**, *34*, 1720–1729.
- (31) Jiang, K.; Su, Y. L.; Xie, B. Q.; Jiang, S. C.; Zhao, Y.; Wang, D. J. *J. Phys. Chem. B* **2008**, *112*, 16485–16489.
- (32) Jiang, K.; Su, Y. L.; Xie, B. Q.; Meng, Y. F.; Wang, D. J. *J. Phys. Chem. B* **2009**, *113*, 3269–3272.
- (33) Xie, B. Q.; Shi, H. F.; Liu, G. M.; Zhou, Y.; Wang, Y.; Zhao, Y.; Wang, D. J. *Chem. Mater.* **2008**, *20*, 3099–3104.
- (34) Liu, G. M.; Xie, B. Q.; Fu, D. S.; Wang, Y.; Fu, Q.; Wang, D. J. *J. Mater. Chem.* **2009**, *19*, 6605–6609.
- (35) Huber, P.; Knorr, K. *Phys. Rev. B* **1999**, *60*, 12657–12665.
- (36) Taggart, A. M.; Voogt, F. V.; Clydsdale, G.; Roberts, K. J. *Langmuir* **1996**, *12*, 5722–5728.
- (37) Fu, D. S.; Su, Y. L.; Xie, B. Q.; Zhu, H. J.; Liu, G. M.; Wang, D. J. *Phys. Chem. Chem. Phys.* **2011**, *13*, 2021–2026.